were 332 msec for v_R of 6 km/hour and 709 msec for v_R of 1 km/hour at a simulated distance of 20 m). Curves fitted to the data (*7*) of both the field and laboratory experiments show for the overlapping range of relative velocities between about 2 and 6 km/hour a mean elevation factor of 3.27 ± 0.50 (range, 2.18 to 4.01) for the times to detect changes in headway under field conditions (Fig. 3).

The thresholds for object-motion detection under simulated conditions were elevated to the level of the vehicle experiment when subjects were simultaneously exposed to an artificial moving visual surround, which induces apparent self-motion, even though the ellipse characteristics remained unchanged. Thus, it is the perception of self-motion—real or apparent—which is responsible for the higher detection thresholds on the road rather than the presence of a textured background per se, which has no effect on the thresholds for object-motion detection (*8*).

During movement in a vehicle, perception of the motion of an object is impaired relative to perception under stationary conditions. Authorities on road traffic accidents evaluating perceptual processes and tolerable reaction times must consider the additional perceptual latencies involved in detecting changes in headway. Typically only the time span between the subjective perception of a critical traffic situation and the initiation of the braking maneuver is considered. Our data, however, also indicate a delay between the onset of the so-called objective stimulus situation (here, the very beginning of the change in headway) and the perceptibility of this event. This delay increases the total reaction time by at least 300 msec (d_o = 20 m, v_R = 19 km/hour, increasing with distance). Fifty percent of auto accidents involving rear end collisions occur with a relative velocity between the involved vehicles of only 19 km/hour (*9*). This interval is further increased by at least 250 msec if a saccadic change of gaze becomes necessary to fixate the potential obstacle (*10*). If a correction saccade is necessary an additional 130 msec is required (*11*).

As a consequence, drivers—particularly during high-density traffic flow—should not rely solely on their movement perception but rather should evaluate the flashing of the brake lights of the vehicle ahead as a trigger for an immediate brake response to minimize their reaction times. Additional brake lights at eye level are recommended to partially reduce these times (*12*). The subsequent control of braking force should be guided by the perception of the change in headway. The estimates of safe following distances should be corrected by taking into account the additional 300 msec required for perception of headway change. This duration must be added to the hitherto acceptable range of reaction times which varies between 0.6 and 1.0 seconds.

THOMAS PROBST
SIEGBERT KRAFCZYK
THOMAS BRANDT
Neurological Clinic Klinikum Grosshadern, University of Munich, 8000 Munich, Federal Republic of Germany
EUGENE R. WIST
Department of Psychology, University of Konstanz, 7750 Konstanz, Federal Republic of Germany

References and Notes

1. E. R. Wist, T. Brandt, S. Krafczyk, *Brain* **106**, 153 (1983).
2. T. Probst and E. R. Wist, *Perception* **11**, A33 (1982).
3. Adequate object-motion perception is also affected by smooth pursuit eye movements as demonstrated by Wertheim [*Acta Psychologica* **48**, 97 (1981)], who asked his subjects to detect the motion of a patterned visual field (background) during concurrent visual tracking of a single object projected onto the moving background.
4. Optokinetic full-field pattern motion induces, after a latency of several seconds, an apparent self-motion opposite in direction to pattern motion, indistinguishable from real self-motion, which is the result of a visual-vestibular convergence [J. Dichgans and T. Brandt, *Handbook of Sensory Physiology*, vol. 8, *Perception*, R. Held, H. W. Leibowitz, H.-L. Teuber, Eds. (Springer, Berlin, 1978), pp. 755–804].
5. D. Degner and T. Brandt, *Pflügers Arch.* **389** (Suppl.) R30, 118 (1981).
6. Linear vection is defined as a perception of linear self-motion induced by a moving visual scene (railway illusion) with a saturation level between 0.8 and 1.0 m/sec [A. Berthoz and J. Droulez, *Tutorials on Motion Perception*, A. H. Wertheim, W. A. Wagenaar, H. W. Leibowitz, Eds. (Plenum, New York, 1982), pp. 157–199.
7. Calculated with SAS (Statistical Analysis System, IBM 370/168 os, Nuclear Research Facility, Jülich, Federal Republic of Germany): nonlinear least-squares grid search.
8. L. O. Harvey and J. A. Michon, *J. Exp. Psychol.* **103**, 317 (1974).
9. A Study by German Motor Traffic Insurers on 28,936 Car Crashes with Passenger Injury [German Association of Third-Party Liability, Accident and Motor Traffic Insurers (HUK-Verband), Hamburg, 1975].
10. T. Uemura, Y. Arai, C. Shimazaki, *Acta Otolaryngol.* **90**, 191 (1980).
11. W. Becker and A. F. Fuchs, *Vision Res.* **9**, 1247 (1969).
12. IIHS Status Report **18**(15), 1 (1983).

10 November 1983; accepted 3 May 1984

Measurement of Myelin Sheath Resistances: Implications for Axonal Conduction and Pathophysiology

Abstract. *As commonly understood, the myelin sheath of axons insulates the internodal axolemma and essentially restricts transmembrane currents to nodal regions. However, recordings obtained from within the myelin sheath showed that its apparent resistance to current generated by action potentials is similar in magnitude to that of the internodal axolemma. This suggests that the sheath does not appreciably limit transmembrane current flow, presumably because there is a longitudinal shunt under the myelin and through the paranodal region. Thus, in some demyelinating diseases and other axonopathies, the safety factor for impulse conduction may be lowered by a loosening or a reduction in the number of paranodal axoglial junctions.*

Our present concepts of impulse conduction in myelinated axons developed from experiments (*1*) that demonstrated the insulating properties of myelin. In particular, the specific radial resistance of the internode was found to be high; its specific capacitance was low; and large inward and outward transmembrane ionic currents were observed only at the nodes. The membrane parameters derived from these studies have since been used in all computer models of impulse propagation along myelinated axons (*2–5*). Since it was not possible to distinguish the biophysical parameters of the two different internodal membranes, the sheath's radial resistance in these models has been assumed to be $2M$ (M being the number of myelin lamellae) times that of the internodal axonal membrane. These models have confirmed results of physiological studies of structure-function relationships (*3*) and have been used to predict the impulse conduction safety factor under conditions of demyelination (*4, 5*). However, the data we report here, together with results obtained by others, indicate that the electrophysiological parameters of the internodal axolemma and its sheath, and the type of cable structure used to represent a myelinated axon, need to be reconsidered.

The morphological correlates of electrophysiologically localized active sites along the goldfish Mauthner axon were investigated (*6*). Except for its lack of typical nodal gaps, the structure-function relationships of the Mauthner axon and its myelin sheath were indistinguishable from those of other central and peripheral nervous system myelinated axons. In these experiments, intrasheath injections of Lucifer yellow or horseradish peroxidase from glass microelectrodes were used to determine the structure of the oligodendrocytes ensheathing

the axon. The position of the electrode deep within the myelin sheath was established by recording a large antidromic action potential (AP), elicited by spinal cord stimulation, in the absence of any significant d-c potential. The electrode position was confirmed by the pattern of dye staining: none was present in the axon, and the dye was distributed throughout cytoplasmic channels within the myelin sheath. In many hundreds of penetrations the largest AP amplitude observed within the sheath was only 80 mV (Fig. 1A1); a more typical value was between 50 and 60 mV. The slightest advancement of the microelectrode then resulted in a jump in d-c potential to −85 mV typically, with a simultaneous increase in AP amplitude to 115 mV (Fig. 1A2). Dye injection at this position confirmed that such recordings were intra-axonal. Significantly, the AP amplitude increased steadily as the sheath was penetrated through a depth of 10 to 20 μm (*7*). This is consistent with recording from a homogeneous resistive structure surrounding the axon and cannot be explained by postulating microelectrode-induced leakage, which would be associated with a very steep and nonlinear AP gradient just outside the axolemma. Intrasheath AP's of comparable size have also been reported in single myelinated fibers of cat (*8*) and frog spinal cord (*9*), lizard and frog peripheral nerves (*9, 10*), and tench and catfish Mauthner axons (*11*). The amplitude ratio of the maximal intrasheath and intra-axonal AP's in this and the cited studies averaged about 1/2. Furthermore, there were no significant differences in the time courses of the extra- and intra-axonal AP's, so circuit capacitances may be ignored in this analysis. These findings thus suggest that the resistance from within the axon to ground is about equally distributed across the internodal axolemma and the sheath (in the extreme case of Fig. 1A the resistance ratio was 1:2).

In order to confirm this conclusion independently and, further, to determine the ratio of longitudinal axoplasmic current to internodal transmembrane current, we measured transfer resistances (i) deep within the Mauthner axon's myelin sheath ($R_{my\text{-}my}$ = 0.58 ± 0.15 megohm, mean ± standard deviation; n = 5) (Fig. 1B2); (ii) across the axolemma ($R_{ax\text{-}my}$ = 0.28 ± 0.08 megohm) (Fig. 1C2); and (iii) within the Mauthner axon ($R_{ax\text{-}ax}$ = 1.3 megohms) (*12*) (Fig. 1D2). An electrical analysis (*13*) indicated that the equivalent resistance of the entire sheath (R_l) was about one-third that across the internodal axolemma (R_c), which again points out the inadequacy of the assumption that $R_l/R_c = 2M$ (≈560 for the Mauthner axon; see below). Furthermore, the combined series resistance ($R_l + R_c$) to internodal transmembrane current is not high, but rather is nearly equal to the combined resistance to ground of all other parallel pathways from an intra-axonal current source (Fig. 2, B and D). Thus, despite the many hundreds of layers of membranes that are stacked on top of one another, the overall effectiveness of the sheath is equivalent to only one or two membranes in series, each having the same specific resistance as the internodal axolemma.

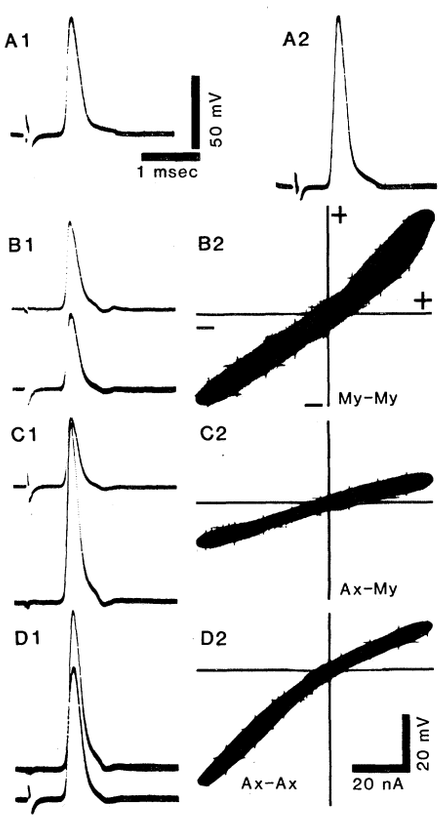

Fig. 1. (A1) Maximal antidromic action potential recorded within the sheath of the goldfish Mauthner axon. Resting potential (RP) = −1 mV. (A2) Intra-axonal recording, obtained after the slightest advancement of the microelectrode from its position in (A1). RP = −87 mV. (B to D) Two independent microelectrodes were used to obtain steady-state voltage recordings (recording 1) and voltage-current relations (recording 2) whose slopes yield transfer resistances (R_t). The oscillographic plots yielding R_t were generated by passing a triangle wave current (1 cycle per 3 seconds) through one electrode (abscissa) while recording the voltage response at the other electrode (ordinate); (+) depolarizing, (−) hyperpolarizing. (B) Both electrodes deep within the myelin sheath (My-My). (B2) R_t = 0.60 megohm. Electrode separation (Δx) = 0.5 mm, or 1/10 space constant. Since R_t decreased when the axolemma was penetrated, the electrodes must be electrically "close" in the sheath, and thus R_t is a fair approximation to the input resistance of the myelin sheath. (C) One electrode (C1, top trace) deep within myelin with other electrode intra-axonal (Ax-My). (C2) R_t = 0.32 megohm; Δx = 0.5 mm. (D) Both electrodes intra-axonal (Ax-Ax). (D2) R_t = 1.00 megohm; Δx = 1.1 mm. R_t can be used to calculate the axonal input resistance [1.3 megohms (*6*)]. Calibrations in A1 apply to all impulses and those in D2 pertain to all R_t plots.

The next issue in understanding AP current flow in myelinated axons is determining how this internodal transmembrane current then divides between the radial resistance of the myelin sheath (R_{my}) (see Fig. 2D) and the various longitudinal periaxonal "leak" pathways (R_{il}). It is useful to consider two extreme possibilities.

1) The myelin sheath is uniformly "leaky." That is, the lamellar membranes have low specific resistance, or there are cytoplasmic channels within or between each lamella that act as low-resistance radial shunt pathways to ground.

2) The major pathway for return current is a longitudinal one through the periaxonal space or the inner cytoplasmic loops of the myelin sheath (or both), to the paranodal region contiguous to the source of action current, and thence into extracellular space. This anatomically prominent pathway (*10*) would effectively shunt current away from the radial path through the myelin membranes.

Regarding the first possibility, with a thickness of at least 5 μm and a periodicity of 18 nm between minor dense lines (*14*), the Mauthner axon myelin sheath consists of 560 membranes constituting 280 lamellae. If sheath input resistance measures the radial resistance across those myelin membranes, each would have a specific resistance of approximately 8 ohm · cm^2 (*6*), an exceedingly low value. Therefore, we think it is unlikely that most of the internodal transmembrane current flows radially and conclude that it is shunted longitudinally, as shown schematically in Fig. 2B. This model is likely to be applicable to other myelinated axons as well. Barrett and Barrett (*10*) concluded that the combined resistance of periaxonal longitudinal pathways in frog peripheral myelinated fibers is about 9 megohms. Thus, although the internodal membranes of those fibers apparently offer a rather high radial resistance of 160 to 255 megohms (*15*), the effective resistance of the sheath to current generated by a propagating action potential appears to be considerably lower than that.

There has been speculation that loosening the seal between the axon and the myelin sheath in the paranodal region could compromise the insulating proper-

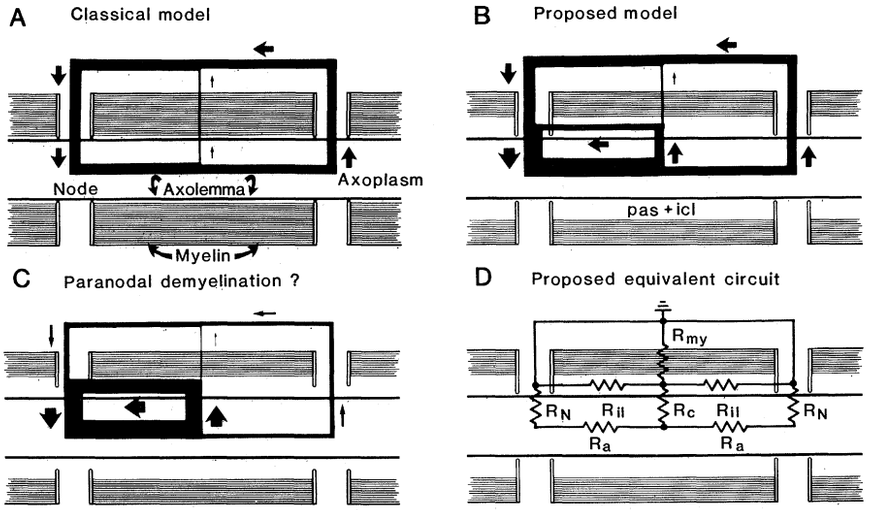

Fig. 2. Schematic representations of action currents flowing through and around a myelinated axon. The internodal sheath (closely spaced parallel lines) surrounds a cylindrical axolemma. An active node is depicted on the left of each diagram with impulse propagation proceeding toward the right. Only the action current loops involving the first downstream internode and node are illustrated. The thickness of the lines and arrows representing the currents suggest relative magnitudes but are not necessarily accurate representations. (A) In the classical view of saltatory conduction, the greater part of the action current entering the axon at the left node passes longitudinally through the axoplasm to the next downstream node, with only minor radial current loss through the sheath. (B) In our proposed model, the radial current through the internodal axolemma is roughly equal to the longitudinal action current reaching the next downstream node. Of the current that passes through the axolemma, some passes radially through the myelin sheath, as in (A), but more flows longitudinally through periaxonal spaces (pas) and inner cytoplasmic loops (icl) of the myelin, to and then through the paranodal region. When viewed externally, models depicted in (A) and (B) are indistinguishable. (C) Scheme for conduction deficits due to paranodal demyelination. If the paranodal axoglial junctions are disrupted, the intrasheath longitudinal resistance will be reduced and will shunt more action current. As less current reaches the downstream node, there is a reduction in safety factor for impulse propagation. (D) Simple electrical circuit diagram of the double cable model (*21*), which represents the models shown in (B) and (C) and which forms the basis for the analysis of Fig. 1. Symbols: R_{my}, resistance of sheath to radial current flow; R_{il}, internodal longitudinal shunting resistance; R_a, axoplasmic resistance; and R_N, nodal membrane resistance.

ties of the myelin sheath and consequently lower the safety factor for impulse conduction (*16*). Our data provide a rationale for this notion and further suggest that even under normal conditions there is a great deal of internodal transmembrane current flow. Since a significant portion of that current is apparently directed back to the paranodal regions, the number or the "tightness" of the paranodal axoglial junctions may be critical in determining the safety factor for impulse propagation. Finally, our proposed model (Fig. 2B) suggests that emphasis should not be placed exclusively on the thickness of the myelin sheath when evaluating the functional role of internodes. In particular, since the internodal axolemma itself appears to be an important barrier to transmembrane current, whereas the radial current flowing through the myelin may be relatively insignificant, altering myelin thickness would be expected to have only minimal effects on the action currents flowing in an axon. This is consistent with clinical observations of deficits in demyelinative pathologies and previous computer modeling (*4, 5*).

In general, the difficulties in correlating pathology with effects on conduction (*4*) may be due to the major consequences of minor changes in the paranodal axoglial junctions (*17*) (Fig. 2C). For example, Uhthoff's symptom (*18*) can occur before any detectable rise in core temperature (*19*) and may thus result from a biochemically induced modification of the paranodal junctions or a metabolically induced local edema that lowers the resistance of the paranodal current pathway. There is supporting evidence for such mechanisms from tissue culture studies in which changes in extracellular calcium result in damage to the paranodal junctions and subsequent accumulation of fluid within the paranodal and periaxonal extracellular spaces (*20*).

PAUL G. FUNCH
DONALD S. FABER
Division of Neurobiology, Department of Physiology, State University of New York, Buffalo 14214

References and Notes

1. A. F. Huxley and R. Stämpfli, *J. Physiol. (London)* **108**, 315 (1949); I. Tasaki, *Am. J. Physiol.* **127**, 211 (1939); *ibid.* **181**, 639 (1955); see reviews in R. Stämpfli, in *Demyelinating Disease: Basic and Clinical Electrophysiology*, S. G. Waxman and J. M. Ritchie, Eds. (Raven, New York, 1981), pp. 11–23; and in I. Tasaki, *Physiology and Electrochemistry of Nerve Fibers* (Academic Press, New York, 1982).
2. R. Fitzhugh, *Biophys. J.* **2**, 11 (1962); W. L. Hardy, *ibid.* **13**, 1071 (1973).
3. M. H. Brill, S. G. Waxman, J. W. Moore, R. W. Joyner, *J. Neurol. Neurosurg. Psychiatry* **40**, 769 (1977); L. Goldman and J. S. Albus, *Biophys. J.* **8**, 596 (1968); N. A. Hutchinson, Z. J. Koles, R. S. Smith, *J. Physiol. (London)* **208**, 279 (1970); J. W. Moore, R. W. Joyner, M. H. Brill, S. G. Waxman, M. Najar-Hoa, *Biophys. J.* **21**, 147 (1978).
4. Z. J. Koles and M. Rasminsky, *J. Physiol. (London)* **227**, 351 (1972); C. L. Schauf and F. A. Davis, *J. Neurol. Neurosurg. Psychiatry* **37**, 152 (1974).
5. R. S. Smith and Z. J. Koles, *Am. J. Physiol.* **219**, 1256 (1970).
6. P. G. Funch and D. S. Faber, *J. Neurophysiol.* **47**, 1214 (1982); P. G. Funch, M. R. Wood, D. S. Faber, *J. Neurosci.*, in press.
7. The Mauthner fiber sheath thickness is about 15 μm. Although care was taken to advance the microelectrode only a few micrometers at a time, determinations of depth of penetration are imprecise.
8. J. W. Woodbury and H. D. Patton, *Cold Spring Harbor Symp. Quant. Biol.* **17**, 185 (1952).
9. I. Tasaki, *Jpn. J. Physiol.* **3**, 73 (1952).
10. E. F. Barrett and J. N. Barrett, *J. Physiol. (London).* **323**, 117 (1982).
11. N. G. Greeff and G. M. Yasargil, *Brain Res.* **193**, 47 (1980); I. Tasaki, S. Hagiwara, A. Watanabe, *Jpn. J. Physiol.* **4**, 79 (1954).
12. P. G. Funch and D. S. Faber, *J. Neurophysiol.* **47**, 1196 (1982).
13. In a π-network, with resistance R_1 from within the sheath to ground, resistance R_2 from within the axon to ground, and a coupling resistance R_c between the axon and the sheath, the following relations hold: input resistance (see legend to Fig. 1B) of the myelin sheath $R_{my\text{-}my} = R_1(R_2 + R_c)/(R_1 + R_2 + R_c)$; axonal input resistance $R_{ax\text{-}ax} = R_2(R_1 + R_c)/(R_1 + R_2 + R_c)$; transfer resistance between axon and myelin $R_{ax\text{-}my} = R_1R_2/(R_1 + R_2 + R_c)$. These equations yield values of $R_1 = 0.71 \pm 0.14$ megohm; $R_2 = 2.61 \pm 1.19$ megohms; and $R_c = 2.64 \pm 0.94$ megohms. In Fig. 2D, $R_1 = R_{il} \parallel R_{my}$, and $R_2 = (R_a + R_N) \parallel (R_c + R_1)$.
14. M. R. Celio, *Brain Res.* **108**, 221 (1976).
15. A specific membrane resistance of 0.10 to 0.16 megohm · cm^2 (*1*) and a 2.04 mm internode (*L*) are assumed [$L = 0.146 \times$ fiber diameter; I. Tasaki, K. Ishii, H. Ito, *Jpn. J. Med. Sci. 3* **9**, 189 (1943)].
16. R. P. Bunge, *Physiol. Rev.* **48**, 197 (1968); A. Hirano and H. M. Dembitzer, in *Physiology and Pathobiology of Axons*, S. G. Waxman, Ed. (Raven, New York, 1978), pp. 65–82; S. G. Waxman, in *Demyelinating Disease: Basic and Clinical Electrophysiology*, S. G. Waxman and J. M. Ritchie, Eds. (Raven, New York, 1981), pp. 169–182.
17. Paranodal demyelination will also lower the effective nodal resistance and raise nodal capacitance, which could lower the safety factor for impulse propagation, as pointed out by M. Rasminsky and T. A. Sears [*J. Physiol. (London)* **227**, 323 (1972)].
18. Uhthoff's symptom is a decrease in visual acuity that manifests itself within minutes after the onset of moderate exercise in patients with optic nerve demyelination; C. E. Moore, in *Multiple Sclerosis. Pathology, Diagnosis and Management*, J. F. Hallpike *et al.*, Eds. (William & Wilkins, Baltimore, 1983), pp. 163–175.
19. J. Selhorst, personal communication. Uhthoff's symptom is often associated with a rise in core temperature, which could produce a conduction block, presumably due to the resulting decrease in impulse duration; that is, less charge is available for discharging the membrane potential [M. Rasminsky, *Arch. Neurol.* **28**, 287 (1973)].
20. W. F. Blank, Jr., M. B. Bunge, R. P. Bunge, *Brain Res.* **67**, 503 (1974).
21. R. E. Taylor, *Bull. Math. Biophys.* **14**, 265 (1952).
22. Supported in part by NIH grant NS 17063. We thank E. Koenig for his critical review of this work, and J. Seiler for secretarial assistance.

11 October 1983; accepted 31 May 1984